Earth, Planets and Space

FULL PAPER

Open Access

Stratospheric gravity wave potential energy and tropospheric parameters relationships over South America: a study using COSMIC-2 and METOP radio occultation measurements

Toyese Tunde Ayorinde[1*], Cristiano Max Wrasse[1], Hisao Takahashi[1], Diego Barros[1], Cosme Alexandre Oliveira Barros Figueiredo[1], Solomon Otoo Lomotey[2], Patrick Essien[3] and Anderson Vestena Bilibio[1]

Abstract

Using COSMIC-2 and METOP radio occultation measurements during the years 2020 and 2021, the study presents the first direct and independent relationship between the potential energy (E_p) in the stratosphere, precipitable water vapour (PWV), tropopause heights (TPH), and cold-point heights (CPH) over South America. The South American continent comprises the tropical region, the Andes Mountain range, and mid-latitude climates. The seasonal mean of the potential energy (E_p), the PWV, and the tropopause parameters height (TPH and CPH) were obtained to investigate the relationship between the stratospheric gravity wave (SGW) E_p and the tropospheric parameters (PWV, TPH, and CPH). Around the Andes Mountains to the east, there is significantly less water vapour (PWV < 10 mm) and a relatively high gravity wave E_p ($E_p > 8$ kJ kg^{-1}). A good correlation of variability was found between the PWV and the lower SGW E_p in summer over the tropical region ($\pm 20^{\circ}$). Generally, good and strong correlations were observed in the summer and spring, with negative/no correlations in the winter in 2020 and 2021. Also, good and strong correlations between SGW, PWV, and TPH were observed in the summer at $20^{o}N - 10^{o}N$ in 2020 and 2021. Our result demonstrated the possibility that convective activity was a major driver of the tropical gravity waves over South America. In the subtropical (30°–40°) region, especially in the winter, the tropospheric parameters make little or no contribution to gravity wave activity in the region. The CPH generally showed a no/negative with SGW over the South American tropics. The SGW activities in the tropical region showed an impact on the structure of the tropopause parameters, which could be a result of the convective activity in this region.

Keywords Radio occultation, COSMIC-2, Stratospheric gravity waves, Tropopause parameters

*Correspondence:
Toyese Tunde Ayorinde
toyese.ayorinde@inpe.br
Full list of author information is available at the end of the article

Graphical Abstract

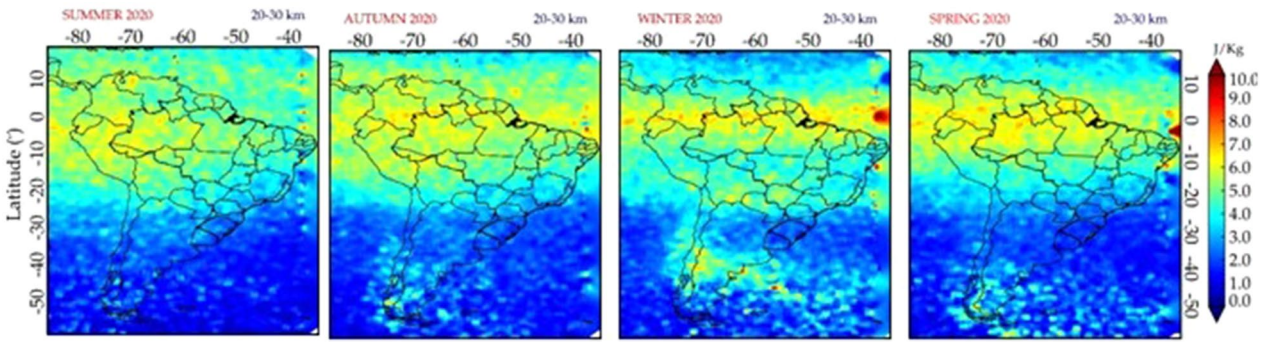

Introduction

Atmospheric gravity waves are critical for large-scale atmospheric circulation, thermal structure, component distributions, transport of chemical constituents to various altitudes, and atmospheric variability from the troposphere to the thermosphere (Son et al. 2011). The atmospheric gravity waves assist in the transportation of atmospheric elements such as water vapour and affect the thermal structure of the tropopause (Xian and Fu 2015; Yu et al. 2019). Due to their critical role in climate dynamics, the upper troposphere and lower stratosphere (UTLS) have recently attracted more interest. The tropopause is the layer separating the upper troposphere and lower stratosphere in terms of vertical mixing durations, trace components, and thermal balance (Son et al. 2011). The gravity waves (GWs) propagate upwards, and their amplitudes increase exponentially due to the exponential decrease in the atmospheric density. GWs break or dissipate in the upper altitudes due to instability or critical level filtering (Fritts and Alexander 2003).

The tropopause's fluctuations, which are caused by changes in the physical, chemical, and thermal features of the troposphere and the stratosphere, are intimately connected to stratosphere-troposphere interchange, as well as climatic variability and change (Schmidt et al. 2008b, a). Tropopause has several definitions and theories (Schmidt et al. 2006). The World Meteorological Organization (WMO) defined the thermal tropopause, also known as the tropopause, as the lowest level at which the lapse rate drops to 2K km^{-1} or less, provided that the average lapse rate between this level and all higher levels within 2km does not exceed 2K km^{-1} (Fueglistaler et al. 2009). The tropopause is derived from vertical profiles of atmospheric temperature and is used internationally, in both the tropics and extratropics (Liu et al. 2014). The cold-point tropopause height is the height at which the minimum temperature occurs when one ascends from the surface to a specific altitude and then rises as one ascends farther into the stratosphere (Randel and Jensen 2013). The cold-point tropopause is a critical parameter for determining stratosphere-troposphere interaction and exchange (Yu et al. 2019). Tropospheric parameters such as height and temperature fluctuations show seasonal and inter-annual variability (Zhou and Holton 2002; Randel et al. 2003; Seidel and Randel 2006) and are closely linked to atmospheric waves (Satheesan and Murthy 2005; Jain et al. 2006), particularly the effects of gravity waves (Das et al. 2010; Khan and Jin 2016).

The relationship between the tropospheric parameters and the stratospheric gravity wave (SGW) potential energy (E_p) has become an important subject since the launch of the Radio Occultation (RO) satellites, especially the Constellation Observing System for Meteorology, Ionosphere, and Climate (COSMIC) satellites. Using the temperature profile from the RO, the GW E_p can be estimated to measure the GW impacts in the atmosphere (Cai et al. 2017; Baumgarten et al. 2018; Yang et al. 2021; Strelnikova et al. 2021; Gisinger et al. 2022). The South American continent comprises different sources of gravity waves, and the peculiar characteristics of these sources and their link with the SGWs have received lesser attention. Even though, there is some research on the changes in tropopause structure (Seidel et al. 2001; Schmidt et al. 2004) and mostly on global SGW activity (Wang and Alexander 2010; Hierro et al. 2012), there are few studies on the interaction between SGWs and the tropospheric parameters, mainly focusing on regional sections like the South American sector. For example, Khan and Jin (2016) studied the connection between SGWs and the temperature and height of the cold-point tropopause and water

vapour over Tibet from June 2006 to February 2014 using the first set of COSMIC RO satellites' temperature data. Their findings indicated a strong association between SGW E_p, cold-point tropopause temperature, and water vapour, and that SGWs affected cold-point tropopause temperature and water vapour concentration in the stratosphere. These studies on the connection between SGWs and the tropopause were mostly regional in scope.

Further analysis is needed on the impact of stratospheric gravity wave activity on the tropopause structure around the globe. Yu et al. (2019) also studied the connection between SGW E_p and tropopause height and temperature around the globe using COSMIC-1 dry temperature profiles from September 2006 to May 2013. They discovered correlation factors between E_p values at various altitudes, and the tropopause height and temperature were estimated correspondingly in each grid. Yu et al. (2019) also found that SGW E_p had a significant positive correlation with lapse-rate tropopause (LRT) height (LRT-H) and a significantly negative correlation with LRT temperature (LRT-T) in the stratosphere, with distinct zonal distribution characteristics at middle and high latitudes. While in the tropics, the distributions of the statistically significant correlation coefficients between SGW E_p and tropopause parameters were dispersive, and the peak correlation was computed across altitudes of 14–38 km.

The second set of COSMIC satellites (COSMIC-2) recently launched provided much higher numbers of occultations than COSMIC-1, at ±40° which provides the opportunity to do a more quantitative and regional study of gravity waves in the stratosphere. The objective of this study is to establish the relationship between the SGWs and the tropospheric parameters, namely, the precipitable water vapour (PWV), the tropopause height (TPH), and the cold-point height (CPH).

Methodology

Observation data

The COSMIC-2 GNSS RO observation produces about 4000 to 5000 RO events per day with high accuracy and precision. RO can obtain more data than the other satellite missions launched previously. On average, COSMIC-2 produces about 15 000–17 000 occultations per month over South America, as obtained from the CDAAC web site (http://cdaac-www.cosmic.ucar.edu/cdaac), providing many chances to study the atmospheric variations on this continent. COSMIC-2 produces different types of products, which include the dry atmospheric temperature profile (atmPrf). The wet atmospheric temperature profile ("wetPrf") is negligibly different from the dry atmospheric temperature profile, the ionospheric profiles ("ionPrf") e.t.c.

The "atmPrf" is an atmospheric profile without moisture information at level-2 of the COSMIC-2 data processed operationally in near-real-time (nrt). A single atmPrf file contains full resolution profiles of physical parameters such as dry pressure, dry temperature, refractivity, bending angle, impact parameters, tropopause parameters (TPH and CPH), and geometric height above mean sea level. One of the leading products in the "atmPrf" is the raw temperature obtained from the COSMIC-2 mission. The COSMIC-2 level 2 "atmPrf" profiles provide dry temperature from the surface to about 60 km, with a vertical resolution of about 1 km in the stratosphere. We noted that COSMIC-1 had a limitation on a relative temperature profile above 45 km due to the symmetric spherical assumption model used in the calculation of the atmospheric refractivity. These errors have been significantly improved in the COSMIC-2 satellites, raising the occultation height up to 60 km, but the limitations are still large above 55 km. Therefore, in this study, an upper limit of 50 km in the stratosphere is used. Figure 1 shows the coverage of temperature profile points available for E_p calculations from COSMIC-2 over South America. Each of the panels shows examples of occultation points for one day (02/Apr/2020), a month (April), a season (summer), and the whole year 2020. These points were used to obtain the E_p.

The gravity wave potential energy

The atmospheric temperature profile ($\boldsymbol{T}$) from COSMIC-2 is a function of height ($\boldsymbol{h}$) which consists of the background temperature profile T (h) and the fluctuating component $\boldsymbol{T'}(\boldsymbol{h})$. The E_p has been used as a proxy for studying the gravity wave activities as presented by Tsuda et al. (2000) is given by:

$$E_p = \left(\frac{g}{N}\right)^2 \left(\frac{\overline{T\prime}}{\overline{T}}\right)^2 \tag{1}$$

where g is the acceleration due to gravity, N is the Brunt-Vaisala frequency, and $\overline{T}$, and $T\prime$ is our background temperature and the temperature fluctuations caused by gravity wave activities, respectively. The E_p calculation is based on the accurate extraction of $T^{'}$, which is given by:

$$T\prime = T - \overline{T} \tag{2}$$

and the N is given as follows:

$$N^2 = \frac{g}{\overline{T}}\left[\frac{\partial \overline{T}}{\partial h} + \frac{g}{C_p}\right] \tag{3}$$

where C_p is the specific heat capacity of air at constant pressure and h is the altitude.

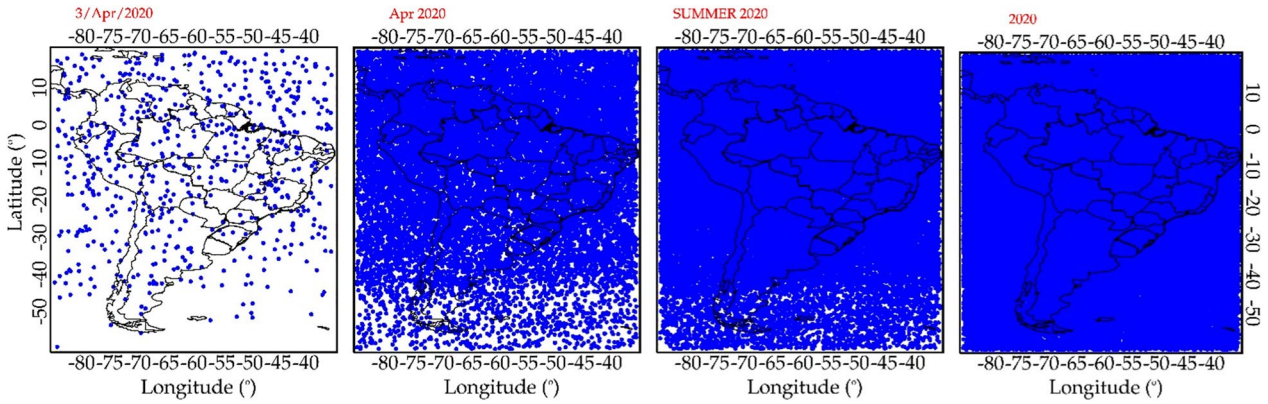

Fig. 1 COSMIC-2 occultation measurements used to calculate the potential energy over South America in 2020. The maps show the coverage of the COSMIC-2 technique over the South American region. The number of occultations for a day (03/Apr/2020), month (April), season (summer), and year (2020) are 645, 18 796, 50.796 and 206.956, respectively

The temperature profile obtained from the COSMIC Data Analysis and Archive Center (CDAAC) is referred to in this paper as the raw temperature profile measured by the COSMIC-2 satellite in the Earth's atmosphere. The gravity wave E_p is calculated using Eq. (1). The E_p depends only on the raw temperature profile, which can be separated into the background temperature ($\overline{T}$), and the temperature fluctuation (T'). In calculating E_p, the $T\prime$ is the main issue that requires careful attention. There are different methods of deriving T'. For example, Hei et al. (2008) used a selected cell size of $20^\circ \times 10^\circ$ of longitude and latitude. They obtained all the available COSMIC-2 data in an individual cell in one month. The mean temperature profiles obtained in each cell are low-pass filtered by using a 4 km vertical running mean to get the T, and later Fast Fourier Transformation (FFT) is applied between 12—33 km of altitude to extract T' with a vertical wavelength shorter than 7 km. De la Torre et al. (2006) used the band-passed filtering method between 4 and 10 km cutoffs. Also, Baumgaertner and McDonald (2007) used a high-pass filter with a Hamming window and a cutoff wavelength of 10 km.

However, the above methods have limitations. They do not remove the influences from the other waves in the atmosphere that are not gravity waves. Scherllin-Pirscher et al. (2021) stated that band-pass filtering is a poor method for separating gravity wave components. Filtering short vertical wavelength fluctuations includes only the gravity waves within the filter band and eliminates the rest of the gravity waves. Short vertical wavelength features include some global-scale waves.

The band-pass method eliminates gravity waves with longer vertical wavelengths. The vertical wavelengths of gravity waves change with height if wind shear is present in the atmosphere. If the intrinsic phase speed (vertical wavelength is proportional to intrinsic phase speed) increases due to changes in the background wind, the band-pass filter naturally removes those gravity waves' vertical wavelength in wind shear. Since winds vary seasonally, the vertical wavelengths will also vary at different seasons. This means that the band-pass filter will automatically filter out the gravity waves with shorter or longer vertical wavelengths depending on seasonal wind changes, and not necessarily make any real changes in the E_p of the gravity waves (Scherllin-Pirscher et al. 2021).

Wang and Alexander (2009, 2010) used the daily COSMIC-1 temperature profiles, which are divided into cell sizes of $20^\circ \times 10^\circ$ of longitude and latitude, between 20 and 50 km of altitude, using a vertical resolution of 0.1 km. The mean temperature profile of each grid is calculated. The Stockwell transform was used to obtain the mean background temperature at each latitude and altitude along the longitude. Also, the zonal wavenumbers between 0 and 6 are obtained using the wavelet transform method to estimate the background temperature (T). The T is interpolated back to the positions of raw the COSMIC-1 profiles and subtracted from the raw temperature profile using Eq. (2) to obtain $T\prime$. The analysis can resolve gravity waves with a vertical wavelength greater than ~2 km, which is twice the vertical resolution of the COSMIC-1 temperature profile data (Wang and Alexander 2009).

In the present study, following the example of Wang and Alexander (2009, 2010), the raw temperature profile obtained from COSMIC-2 is first interpolated to 100 m intervals along the altitudes. Each temperature profile is divided into cells of $20^\circ \times 10^\circ$ of longitude

and latitude between 10 and 50 km of altitude, and the mean temperature of each grid is calculated. The mean temperature profile is decomposed using a continuous wavelet transform (CWT) to obtain the background temperature (T). The T is interpolated back to the positions of temperature profiles and subtracted from the raw temperature profile using Equation (2) to obtain T'.

Precipitable water vapour content

The COSMIC-2 "wetPrf" provides multiple levels of precipitable water pressure data. The specific humidity is easily calculated by water vapour pressure, and air pressure, using Equation (4) (Wang and Zhang 2008). The average specific humidity is calculated by taking the bottom layer specific humidity and the top layer specific humidity given in Equation (5).

$$q = \frac{\varepsilon e}{p - (1 - \varepsilon)e} \tag{4}$$

The mean specific humidity is given as:

$$\overline{q} = \frac{q_{h,i-1} + q_{h,i}}{2} \tag{5}$$

where ε is the constant of the ratio of the molecular weight of precipitable water to dry air, which equals 0.622, e is the precipitable water pressure, p is the total atmospheric pressure, and q is the specific humidity.

To calculate the PWV value from a single wet profile, the specific humidity of each height is integrated from the surface to the retrieved maximum height, using Eq. (6).

$$PWV = \frac{1}{\rho g}\int_{0}^{P_s} q dp = -\frac{1}{g}\sum_{P_s}^{0} q\Delta p \tag{6}$$

In Eq. (6), PWV value in *mm*, Ps is the surface air pressure, g is the value of acceleration due to gravity, q is the specific humidity, and the ΔP is change in pressure. The PWV is calculated to compare with the gravity wave E_p in the stratosphere to study the connection between the gravity wave activities and the deep convection.

Statistical method

In order to see a clear relationship and correlations between the E_p and the tropospheric parameters, the two parameters are normalized with the same scale using the mean normalization formula according to Abraham et al. (2018, p. 400), given in Equation (7). The mean normalization method returns values between -1 and 1, enabling the comparison and correlation of the gravity wave E_p and the tropospheric parameters.

$$x\prime = \frac{x - \mu}{\max(x) - \min(x)} \tag{7}$$

where $x\prime$ is the normalized value of x, the μ is the mean value of x, and x is the original value of E_p and the tropospheric parameters. Also, the correlation coefficients between the SGW E_p and the tropospheric parameters in the tropical, subtropical, and extratropical regions were calculated. The correlation measures the strength of the relationship between variables and is a scaled measure of their covariance. The relationship between the two concepts can be expressed using the following Equation:

$$r(X, Y) = \frac{Cov(X, Y)}{\sigma_X \sigma_Y} \tag{8}$$

where $r(X, Y)$ is the correlation between the variables X and Y, $Cov(X, Y)$ is the covariance between the variables X and Y, σ_X is the standard deviation of the X-variable, and σ_Y is the standard deviation of the Y -variable.

Results

Temperature profiles obtained from COSMIC-2 measurements over South America (30°W - 85°W and 20°N - 60°S) were used to study the SGW activity in 2020. The goal of this research is to demonstrate how SGWs influence tropopause parameters as well as investigate the effect of precipitable water vapour on SGWs. SGWs have an important role in controlling stratospheric water vapour by producing mean updrafts or fluctuating tropopause parametric structures. The results are presented in the altitude range of 20 to 50 km for COSMIC-2 profiles to minimize the errors. The COSMIC-2 satellites measure up to an altitude of 60 km, but as stated by Schreiner et al. (2020) errors due to the symmetric spherical assumption modeling have been significantly improved in the new COSMIC-2 satellites. However, the errors are still large above the altitude of 55 km. Subsequently, in this section, the latitudes will be divided into the following ranges: (1) 20°N–10°N, 10°N–0°, 0°–10°S, 10°S–20°S, and 20°S–30°S are the tropical regions; (2) 30°S–40°S is the subtropical region.

The SGW E_p in Figs. 2 and 3 is divided into three segments: (1) the lower stratosphere (20–30 km); (2) middle stratosphere (30–40 km); and (3) the upper stratosphere (40–50 km). These segments have peculiar characteristics according to the mixing of air in these regions (Salby 1996). Also, the seasons are categorized as summer (December–January–February), autumn (March–April–May), winter (June–July–August), and spring (September–October–November). Tables 1 and 2 present the Pearson correlation coefficients of SGW with the PWV and the tropopause parameters in the tropics and over

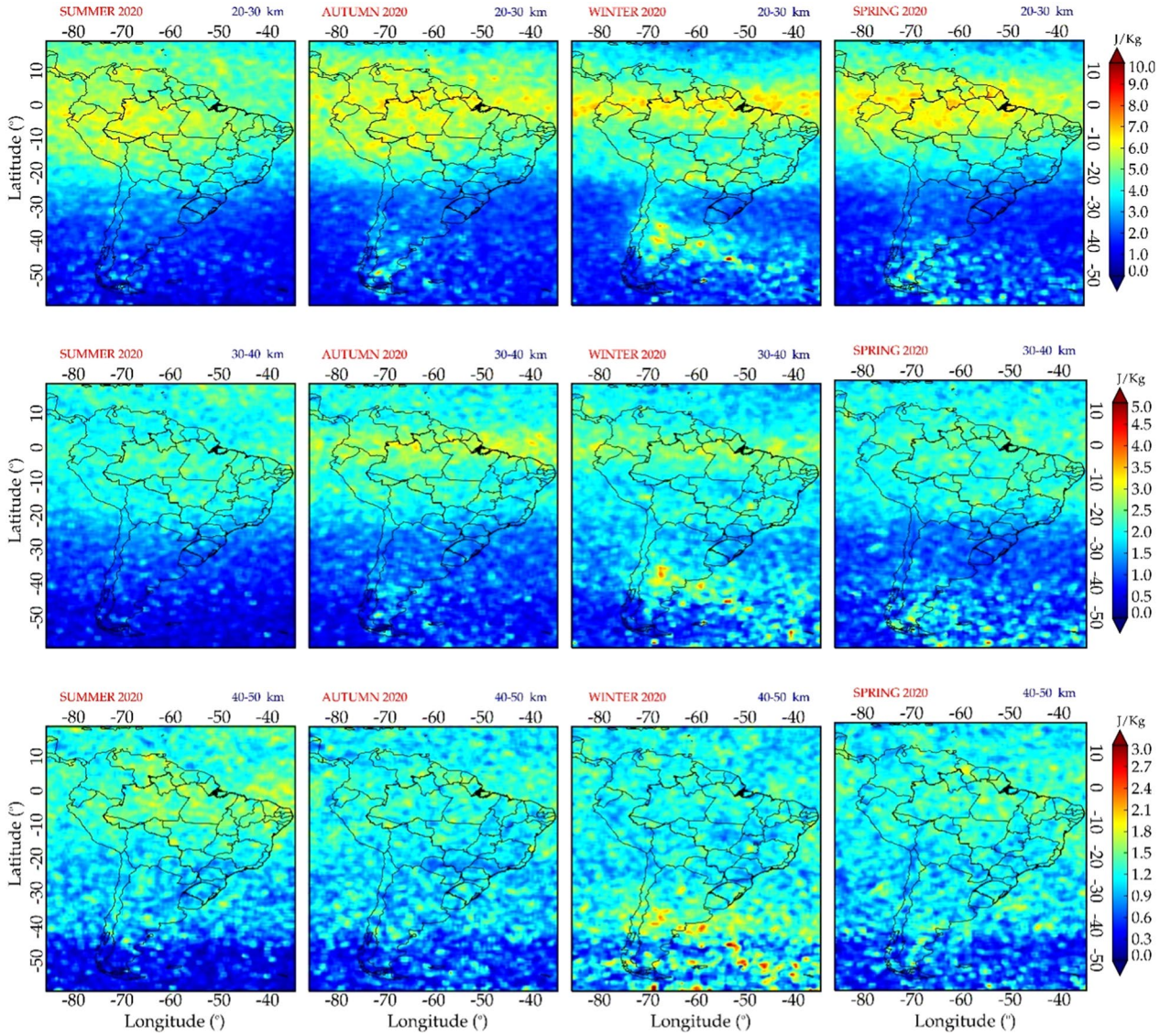

Fig. 2 Seasonal variation of E_p over South America using COSMIC-2 measurements in 2020. The seasonal variation of E_p at 20–30 km, 30–40 km, and 40–50 km are shown at the top, middle, and bottom row, respectively. Each panel has its corresponding labeling at the top. Each row has a corresponding color bar

the Andes Mountain range, respectively, in 2020 and 2021.

Potential energy climatology

The potential energy (E_p) is an efficient parameter to study the gravity wave activities in the atmosphere (e.g.,Tsuda et al. 2000; Schmidt et al. 2004, 2008a). Figures 2 and 3 show the climatology of the SGW E_p over South America for the years 2020 and 2021. It is observed that the SGW E_p for the years 2020 and 2021 showed a similar pattern. The SGW E_p over South America in the summer of 2021 showed higher values than in 2020 at around ±10°. At the lower stratosphere (Figs. 2 and 3, 20–30 km), it can be seen that the gravity wave E_p values range from 6 to 10 J kg^{-1} in the equatorial region (±30°) for all the seasons. In this region, it is observed that the E_p is higher in autumn ±10° latitude around the equator. In the middle stratosphere, it is observed that the E_p has higher values (Figs. 2 and 3) in autumn around the equatorial region.

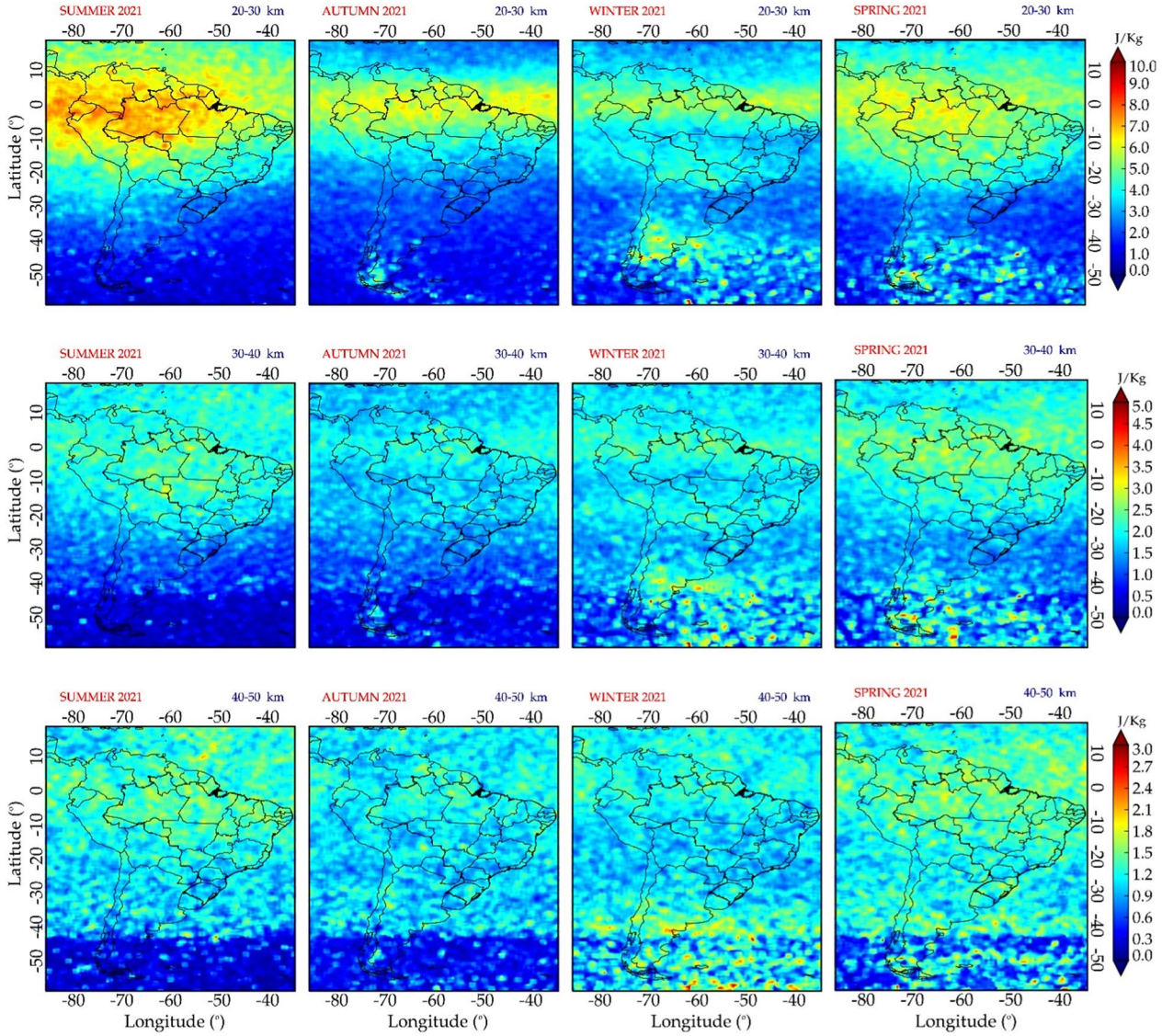

Fig. 3 Seasonal variation of E_p over South America using COSMIC-2 measurements in 2021. The seasonal variation of E_p at 20–30 km, 30–40 km, and 40–50 km are shown at the top, middle, and the bottom row, respectively. Each panel has its corresponding labeling at the top. Each row has a corresponding color bar

The convective activities are more intense in the equatorial region, which could be responsible for the increase in gravity wave E_p values, leading to more SGW activity. There is also evidence of the effect of the wind in the tropical region, called the Northeast and Southeast trade winds, as the gravity waves appear to be more prevalent at higher latitudes. This result agrees with what was reported by Tsuda et al. (2000). Xu et al. (2017) found that the distributions of gravity wave E_p over 20–30 km exhibited similar seasonal and spatial variations compared to our result. In the tropics, the gravity wave E_p is symmetric to the equator in autumn and spring. The distribution of gravity wave E_p around tropical latitudes corresponds to deep convection, which is the principal cause of gravity waves across tropical latitudes (Ratnam et al. 2004).

In the middle stratosphere (30–40 km), there is higher gravity wave activity near the equator in autumn in the middle stratosphere than in other seasons in 2020, and much less in 2021. The gravity wave activity is low (maximum 5 J kg^{-1}) compared to the lower stratosphere (maximum 10 J kg^{-1}). It is also observed that the gravity wave E_p in winter increases from the lower to the upper

Table 1 The correlation coefficient between Ep and the tropopause parameters at 20° N—20° S at 10° intervals (tropical regions) over South America

	OVER THE TROPICAL REGIONS															
	DJF				MAM				JJA				SON			
	Lat1	Lat2	Lat3	Lat4	Lat1	Lat2	Lat3	Lat4	Lat1	Lat2	Lat3	Lat4	Lat1	Lat2	Lat3	Lat4
PWV 2020	0.74	-0.22	0.82	0.5	0.61	0.3	0.62	-0.44	0.48	-0.57	-0.43	0.11	0.83	0.43	0.77	0.26
PWV 2021	0.89	0.18	0.94	0.63	0.56	-0.34	0.1	0.37	-0.21	-0.09	0.25	-0.01	0.52	0	0.92	0.66
TPH 2020	0.79	0.75	-0.46	0.59	0.39	-0.1	-0.21	0.08	-0.29	0.33	0.29	-0.12	0.73	0.61	0.03	0.64
TPH 2021	0.82	0.81	0.57	0.04	0.6	-0.1	0.06	0.13	0.2	0.06	0.28	0.44	0.55	0.66	0.65	0.56
CPH 2020	0.22	-0.4	-0.68	-0.77	0.04	-0.09	-0.27	-0.53	-0.7	0	0	-0.01	0.49	-0.23	-0.61	-0.27
CPH 2021	0.63	-0.66	-0.71	-0.83	-0.02	-0.33	-0.48	-0.63	-0.16	0.1	0.14	0.74	-0.25	-0.61	-0.71	0.08

The latitude ranges are denoted as follows: Lat1 is $20^{o}N - 10^{o}N$, Lat2 is 10° N—0°, Lat3 is 0°—10° S, and Lat4 is 10° S–20° S. The seasons are divided into summer (DJF) overlaid in light yellow color, autumn (MAM) overlaid in light green color, winter (JJA) overlaid in sky blue color, and spring (SON) overlaid in peach color

Table 2 The correlation coefficient between Ep and the tropopause parameters over the Andes region (at 20°S–40°S at the interval of 10° and 65°W–80°W)

	OVER ANDES							
	DJF		MAM		JJA		SON	
	Lat5	Lat6	Lat5	Lat6	Lat5	Lat6	Lat5	Lat6
PWV 2020	0.38	-0.67	-0.63	0.13	0.43	-0.64	0.43	0
PWV 2021	0.78	-0.64	0.33	-0.25	-0.57	-0.74	0.81	0.26
TPH 2020	0.79	-0.42	0.68	0.52	-0.09	-0.78	0.88	0.81
TPH 2021	0.91	0.75	0.29	0.42	0.62	-0.35	0.88	0.62
CPH 2020	0.54	0.9	0.71	0.63	-0.18	-0.06	0.11	0.17
CPH 2021	-0.01	-0.24	0.16	-0.17	0.59	0.8	0.32	0.37

The latitude ranges over the Andes are denoted as Lat5 is 20°S–30°S and Lat6 is 30°S–40°S. The seasons are divided into summer (DJF) overlaid in light yellow color, autumn (MAM) overlaid in light green color, winter (JJA) overlaid in sky blue color, and spring (SON) overlaid in peach color

stratosphere (20–50 km) over the Andes and the Patagonian mountains. This can be attributed to the increase in zonal wind speed, which aids the increase in SGWs activity (Alexander et al. 2009).

The gravity wave activity decreased significantly in the upper stratosphere in the tropical region compared to the lower stratosphere. In spring, the E_p in the tropics declined with height to ~50% across the altitude ranges [~ 3.5 J kg^{-1} in the middle stratosphere and ~1.5 J kg^{-1} in the upper stratosphere (40–50 km)]. It is also noted that the gravity wave E_p values remain unchanged from the middle to the upper stratosphere in the summer. This consistency in the gravity wave E_p values from the middle to the upper stratosphere shows that the gravity waves are not likely subjected to wave dissipation. The high gravity wave activity in the narrow band at ±20° in the lower stratosphere is seen to spread towards the higher latitudes towards the southern hemisphere in the upper stratosphere. Gravity wave activities can also be seen around the equator in the summer, spring, and winter below 40°S.

Seasonal variation of SGW Potential energy

To further describe the seasonal variability of SGWs E_p is presented in Fig. 4, at each latitudinal distribution (20 ° N–10 ° N, 10 ° N–0 °, 0 °–10 ° S, 10 ° S–20 ° S, 20 ° S–30 ° S, and 30 ° S–40 ° S), in the stratosphere for the years 2020 and 2021. The SGWs E_p latitudinal distribution for both years is very similar in both tropical and subtropical regions. Our result showed that ± 20° in the tropical region accounts for most of the SGW activities (~45 to 50%, ± 10° account for ~30 to 35%, of the total mean SGW E_p) in the lower stratosphere (Fig. 4, left panel), which seemed to be clear evidence of convective activities in the tropical region. The increase in the total mean SGW E_p decreased to ~15 to 20% in the upper stratosphere. We suggest this could be a result of the gravity wave filtering. It is important to note that the amplitude of the gravity waves increases with an exponential decrease in the atmospheric density.

20°S–30°S account for ~10 to 13% of the total mean SGW E_p with the highest percentage in the winter (13%) in the lower stratosphere. The SGW activity increases

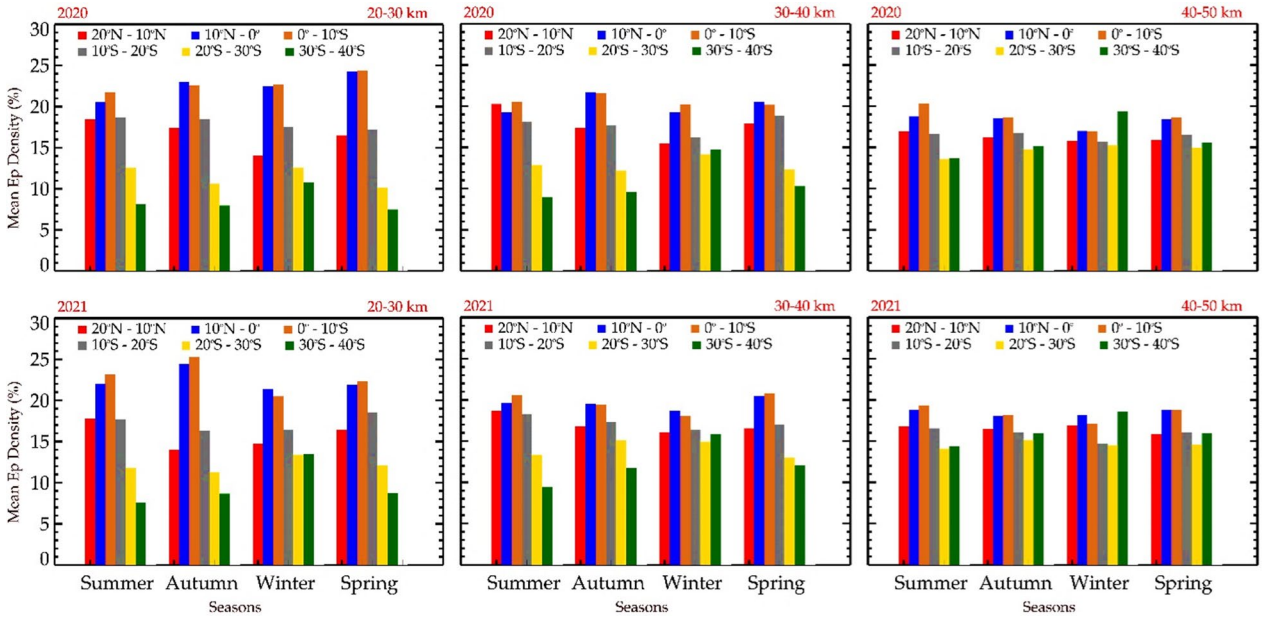

Fig. 4 Seasonal and latitudinal distribution of mean E_p in the stratosphere (in %) in the altitude range of 20–30 km, 30–40 km, 40–50 km during 2020 and 2021. The left panel shows the mean E_p at 20–30 km, the middle panel shows the mean E_p at 30–40 km, and the right panel shows the mean E_p at 40–50 km. The color bars indicate latitudinal zone of 20°N-10°N (red), 10°N-0° (blue), 0°-10°S (chocolate), 10°S-20°S (gray), 20°S-30°S (gold), 30°S-40.°S (dark green)

in the middle stratosphere (~12 to 15%), in the upper stratosphere (~15 to 20%), and also increases in the middle and upper stratosphere (Figs. 3 and 4). This could be the contribution of the mountain waves generated by the extension of the Andes Mountain range (in the winter) combined with the convective activities in the Amazon Rainforest region (in the summer and spring). A consistent increase in SGW activities is seen in the total mean SGW E_p percentage at 30°S–40°S across 2020 from the lower to upper stratosphere, which is more conspicuous in the winter and spring (Fig. 4).

Precipitable water vapour content

The PWV over South America for 2020 and 2021 is shown in Fig. 5. The PWV pattern over South America in both years is seen to be very similar. The PWV is concentrated in the tropical region and mostly at ±10° in all seasons. The PWV in the summer and autumn is higher in the tropics. It is observed that the PWV is higher in the summer and lower in the winter. Most of the PWV is over land, especially over the Amazon rain forest. The western Andes showed no PWV due to the air movement over the Andes Mountains.

There is a lower amount of PWV (25–50 mm) in the southward subtropics (20°–40°S) with PWV lowest in the winter. The extratropical region showed little or no PWV, particularly in the winter. These observations are in good agreement with the results of Hierro et al. (2012); Teng et al. (2013); Zhang et al. (2018). The average PWV reaches a maximum value of 70 mm or more in tropical areas and then decreases to nearly 0 mm in the 40°S–60°S region (mainly in winter). The regional and seasonal variability of PWV is strongly linked to the sources of water vapour and as a direct heat of surface temperature (Zhang et al. 2018). The detailed analyses of the relationship between PWV and the SGW E_p are discussed in the sections below.

Tropopause parameters

The tropopause and the cold-point height are given in the "global attributes" of the "netcdf" files of the COSMIC-2 and METOP RO data. In this study, we focus only on the tropopause and cold-point tropopause heights. Subsequently, the tropopause height is designated as TPHwhile the cold-point height is designated as CPH. According to the WMO's definition, the tropopause height (TPH) is the height at which the temperature variation is not more than 2 K within 2 km between the troposphere and the stratosphere. The cold point tropopause is the coldest region that demarcates the thermal boundary between the troposphere and stratosphere. The cold-point's thermal properties have been studied in-depth due to their importance in troposphere-stratosphere coupling and exchange (Randel et al. 2003). Figures 6 and 7 show that the TPH and the CPH in 2020 and 2021 have a similar trend and an average height of ~17 km

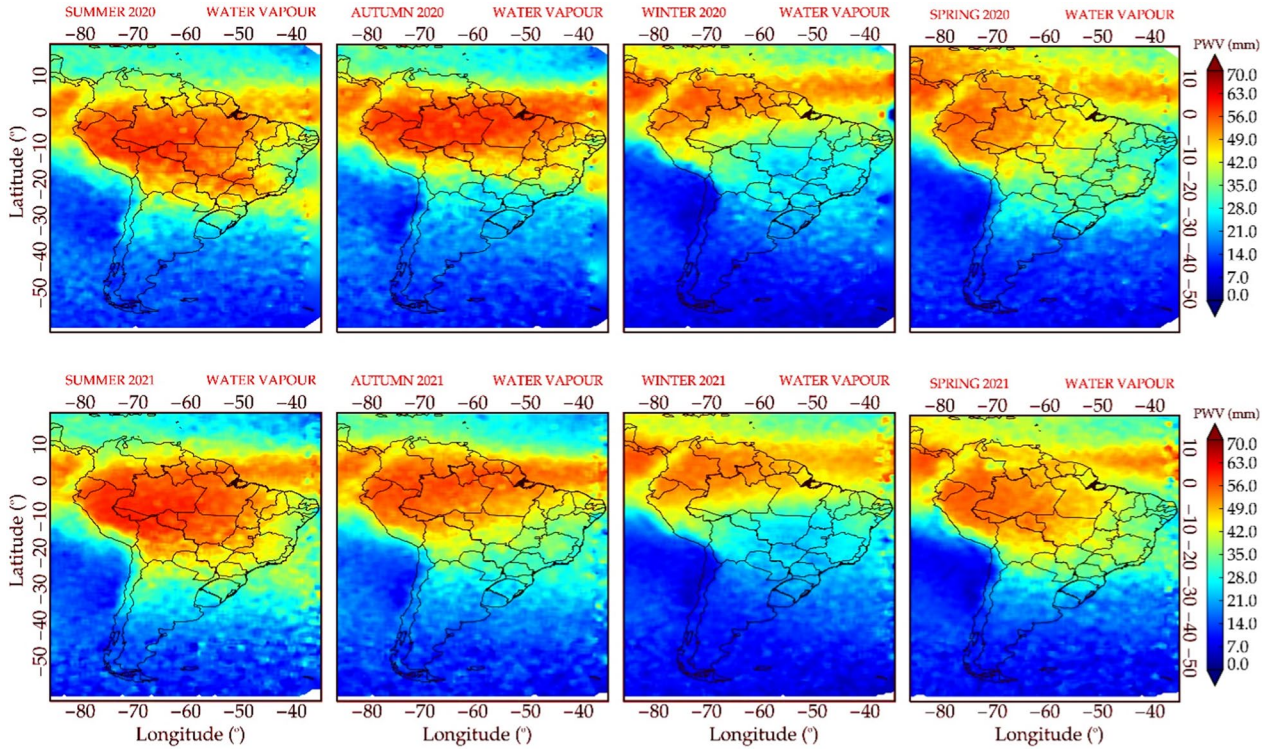

Fig. 5 Seasonal variation of the PWV content over South America in 2020 and 2021. The corresponding labeling is at the top of each panel with the corresponding color bar

at ± 30°. The CPH showed higher variability trend and ~5 km difference from the TPH at 30°S–60°S. This suggests that the WMO's definition of the tropopause is more valid in the equatorial regions. The tropopause and the cold-point height variability at the equatorial region (± 30°) appeared to be more consistent than at the higher latitudes. It is also observed that at higher latitudes (40°S–60°S), the CPH is about 5—10 km higher than at TPH in all seasons. The height of the tropopause is about 5 km higher in tropical areas than in middle latitudes in both summer and winter (Seidel and Randel 2006; Schmidt et al. 2008b). An average gap in the TPH at ~30°S to 40°S and ~40°S to 50°S (Figs. 6 and 7) is noticed to be ~5 km and ~3 km respectively, at the same latitudinal ranges in all the seasons. The change in temperature and height can be explained by the boundary between the Hadley cell and the Ferrel cell in the atmospheric air circulation, which varies monthly and seasonally. Hadley cell and Ferrel cell are two of the cells involved in global air circulation. In the Hadley cell, low-latitude overturning circulations occur with air rising near the equator and sinking at about 30° latitude. They are in charge of the trade winds in the tropics as well as low-latitude weather patterns. Also, in the Ferrel cell (30°–60° in the north and southern hemisphere), air flows poleward and eastward near the surface and equatorward and westward at higher elevations; this movement is the inverse of the airflow in the Hadley cell. The Ferrel cell is the average motion of air in the mid-latitudes that occurs in higher latitudes (Held and Hou 1980). The air parcels blow warm air towards the equator in the Hadley cell. Hence, the tropopause and cold point heights are achieved at lower temperatures at high altitudes (Reid and Gage 1981).

In autumn and winter in 2020, the cold point altitudes are higher, closer to the lower end of the Ferrel cell. In spring, the cold point altitudes are higher, closer to the boundary of the Hadley cell (Randel et al. 2000). The CPH in the Hadley cell followed the same trend as the TPH in the Hadley and Ferrel cells. The tropopause and cold point heights (Figs. 6 and 7) exhibit the same characteristics in summer and spring and the opposite in autumn and winter. It is observed that the tropopause altitudes are higher in the summer and lowest in the winter in the Hadley cell. There are no apparent changes to the tropopause in the Ferrel cell. This result agrees with the findings of Schmidt et al. (2004) and Kishore et al. (2006). The CPH characteristics have been classified as intraseasonal variabilities correlated with tropical convective activity (Zhou and Holton 2002; Randel et al. 2003; Randel and

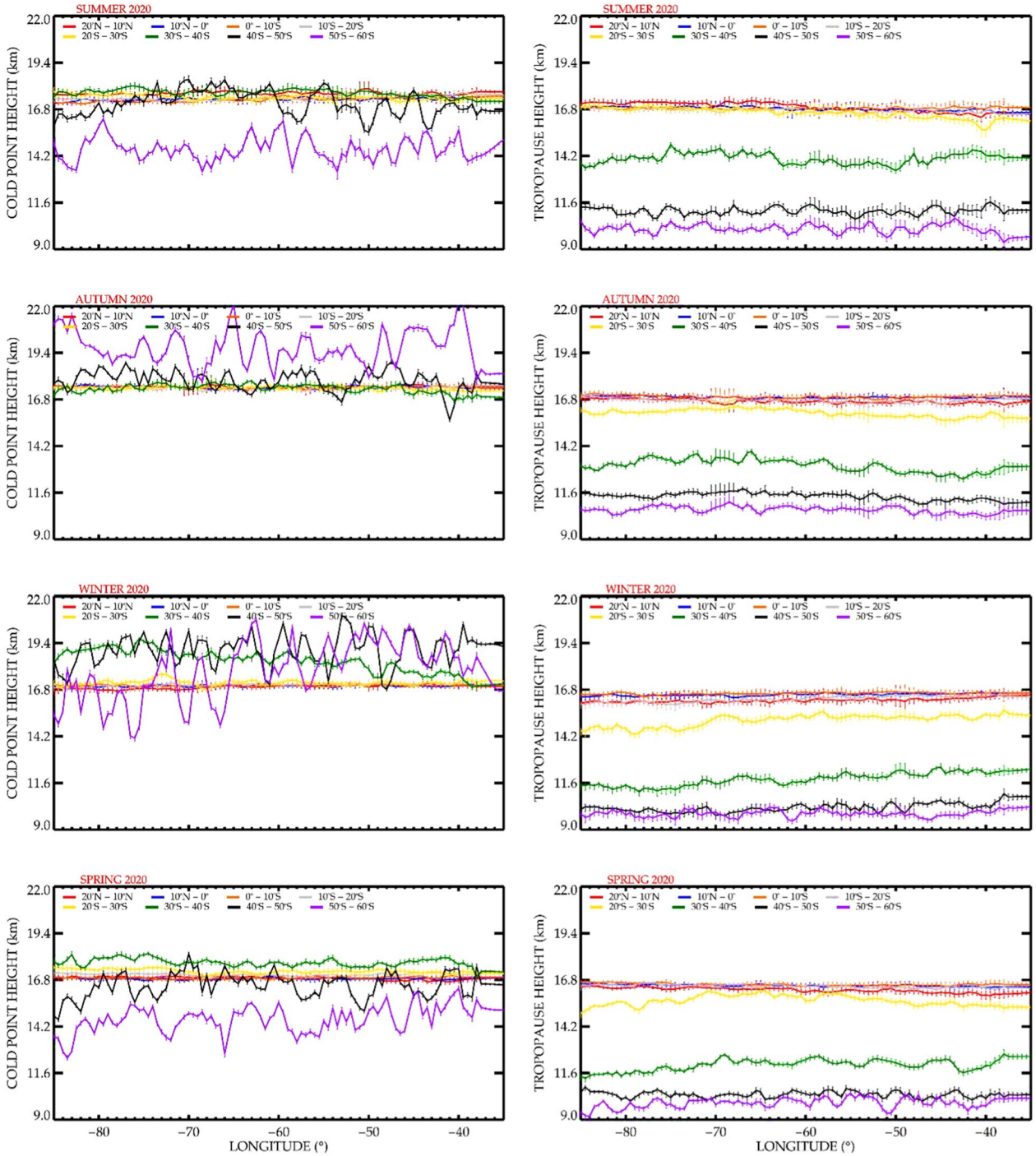

Fig. 6 Latitudinal and seasonal variation of the tropopause height (TPH) and the cold-point tropopause height (CPH) over South America in 2020 with the error bars. The right panels show the TPH, and the left is the CPH. The parameters are plotted over the South American map with the corresponding labeling at the top of each figure. The line color indicates latitudinal zone of 20°N-10°N (red), 10°N-0° (blue), 0°-10°S (chocolate), 10°S-20°S (gray), 20°S-30°S (gold), 30°S-40°S (dark green), 40°S-50°S (black), 50°S-60.°S (purple)

Wu 2005). The detailed analyses of the relationship of the tropopause parameters with the SGW E_p in the tropics and over the Andes region are discussed below.

Potential energy vs tropospheric parameters in the tropics

In this section, we analyzed the latitudinal variation of SGW E_p and the tropospheric parameters (PWV, TPH,

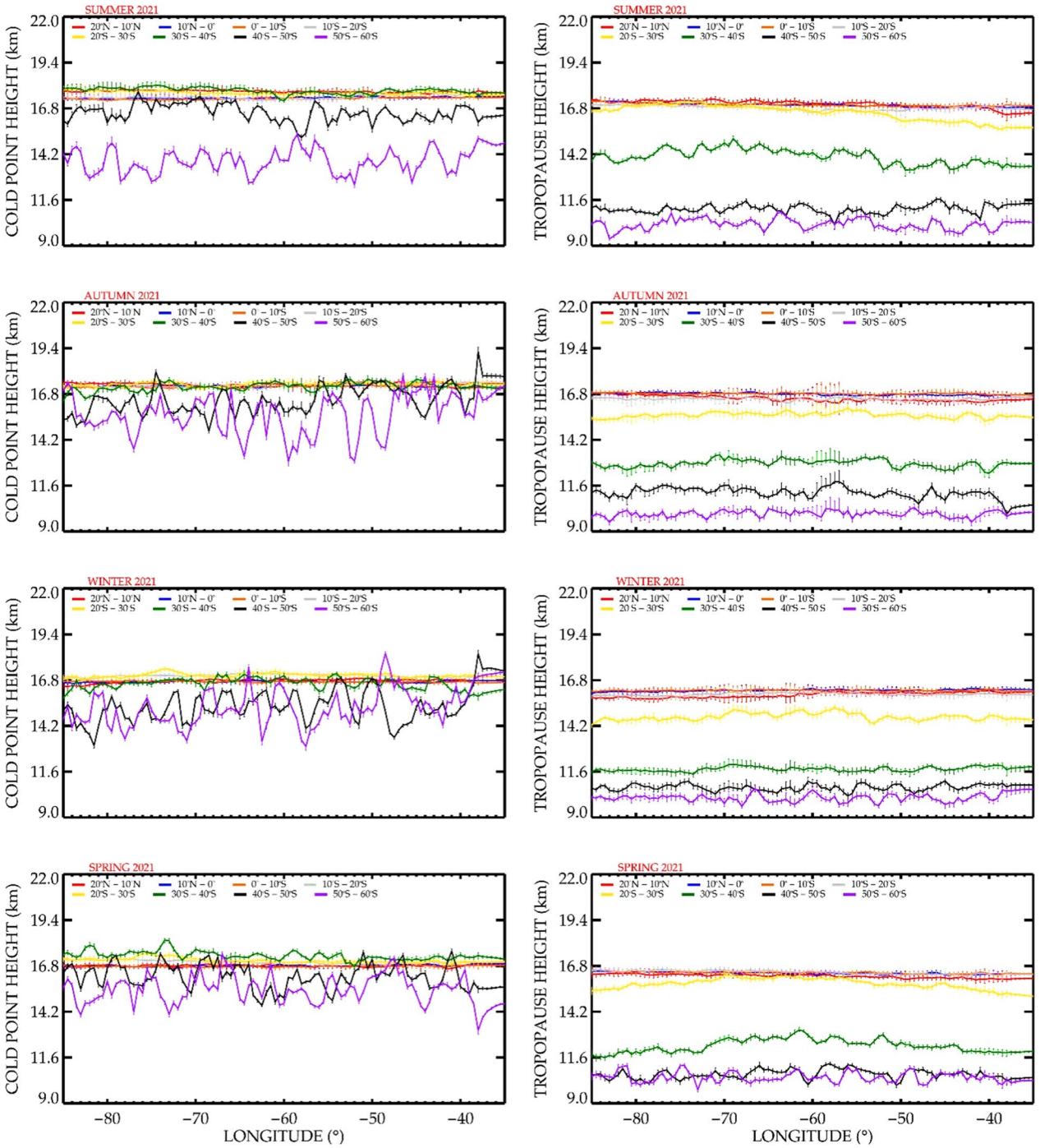

Fig. 7 Latitudinal and seasonal variation of the tropopause height (TPH) and the cold-point tropopause height (CPH) over South America in 2021 with the error bars. The right panels show the TPH, and the left is the CPH. The parameters are plotted over the South American map with the corresponding labeling at the top of each figure. The line color indicates latitudinal zone of 20°N-10°N (red), 10°N-0° (blue), 0°-10°S (chocolate), 10°S-20°S (gray), 20°S-30°S (gold), 30°S-40°S (dark green), 40°S-50°S (black), 50°S-60.°S (purple)

and CPH) and their respective correlation coefficients in the tropics during the years 2020 and 2021. The latitudinal ranges are divided into four, namely: 20°N–10°N, 10°N–0°, 0°–10°S, 10°S–20°S. In this section, the acronyms for the latitudinal ranges in Tables 1 and 2 are defined as follows: Lat1 is $20°N - 10°N$, Lat2 is 10 ° N -0, Lat3 is 0–10 ° S, Lat4 is 10 ° S–20 ° S, and in Table 2, the latitude ranges over the Andes are denoted

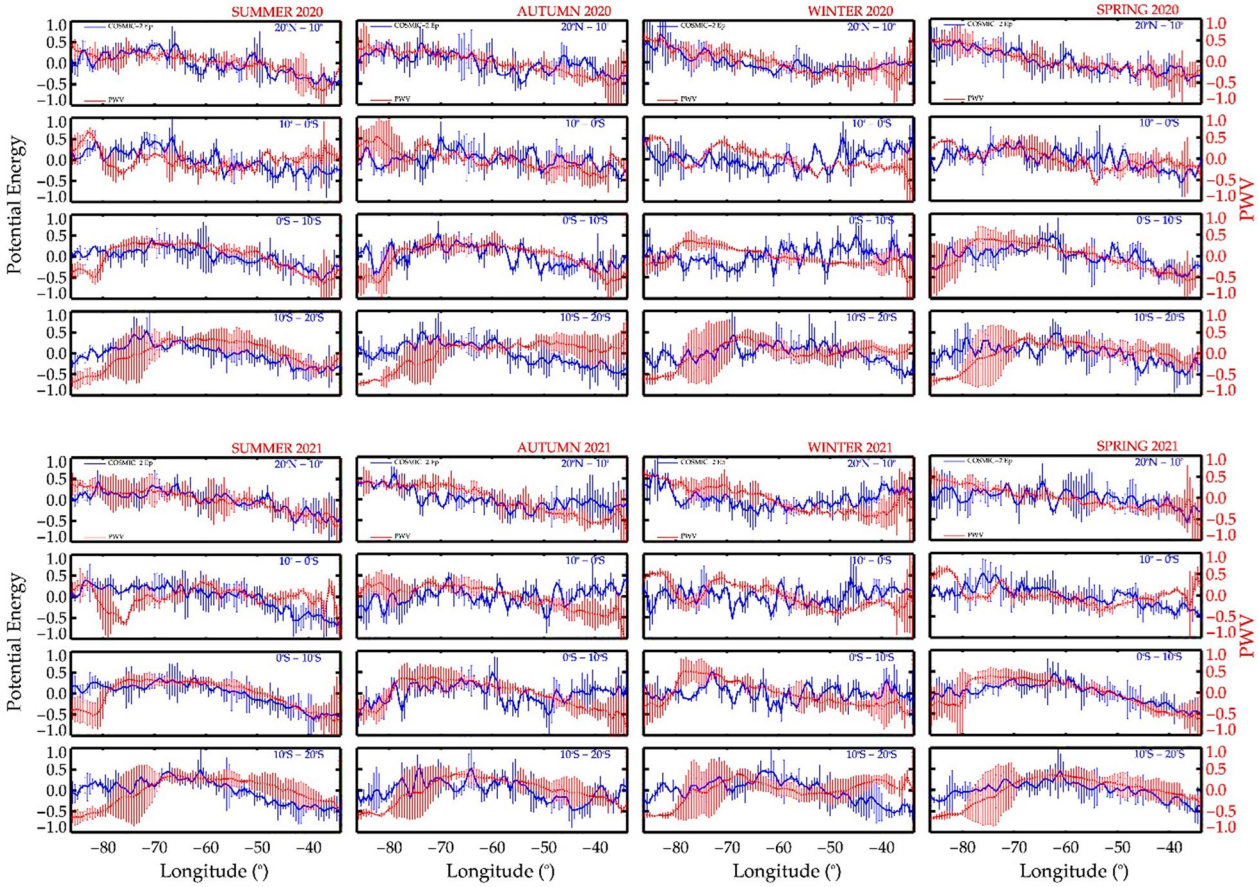

Fig. 8 The seasonal relationship between the latitudinal mean normalized E_p distribution (blue line) and the water vapour (PWV) (red line) with the error bars for 20°N–10°N, 10°N–0°, 0°–10°S, 10°S–20°S at 2020 and 2021. Each panel shows the mean E_p distribution and the PWV at 20–30 km altitude

as Lat5 is 20 ° S–30 ° S and Lat6 is 30 ° S–40 ° S. Figure 8 shows the relationship between the normalized SGW E_p and PWV at the four different latitudinal regions (20 ° N–10 ° N, 10 ° N–0, 0–10 ° S, 10 ° S–20 ° S). In this section, the correlation coefficients are categorized as negative/anticorrelation correlation strong negative/anticorrelation if $r < -0.6$, good negative/anticorrelations if $-0.3 > r > -0.6$; weak negative correlation if $-0.1 > r > -0.3$; and no correlation if $0 < r < 0.1$. The positive correlation coefficients are categorized as weak positive correlation if $0.1 < r < 0.3$, good positive correlation if $0.3 < r < 0.6$, and strong positive correlation if $r > 0.6$. Figure 9 also shows the relationship between the normalized SGW E_p, TPH, and CPH at the same four different latitudinal regions. Tables 1 and 2 show the correlation analysis over the tropical region and the Andes Mountain range. For easy identification, we divided the seasons into summer (DJF), autumn (MAM), winter (JJA), and spring (SON) and overlaid them with light yellow, light green, sky blue, and orange colours, respectively. In general, positive correlations of PWV and TPH with SGW were found mostly in the summer and spring, with an anticorrelation ($r < 0$) no correlation, or weak correlation ($r <\sim 0.3$) in the winter in all the latitudinal ranges in 2020 and 2021. Some exceptions were noticed at Lat2 (10°N–0°N), where the correlation between PWV and SGW was negative ($r = -0.22$) in summer, and weak ($r = 0.18$) in summer, and no correlation ($r = 0$) in spring in 2021. These exceptions could be a result of non-regular tropospheric occurrences like frontal systems (Hierro et al. 2012) or equatorial oscillations (Yu et al. 2019). Figure 8 shows that the SGW Ep and PWV have a similar trend along the seasons in the latitudinal range of 20°N–20°S. The relationship between convection and the thermal structure of the upper troposphere has been linked with warm anomalies in the upper troposphere and cold anomalies at the tropopause (Kim and Son 2012; Xian and Fu 2015; Yu et al. 2019).

Figures 8 and 9 showed similarities in the trend between the SGW E_p and PWV. Although this similarity

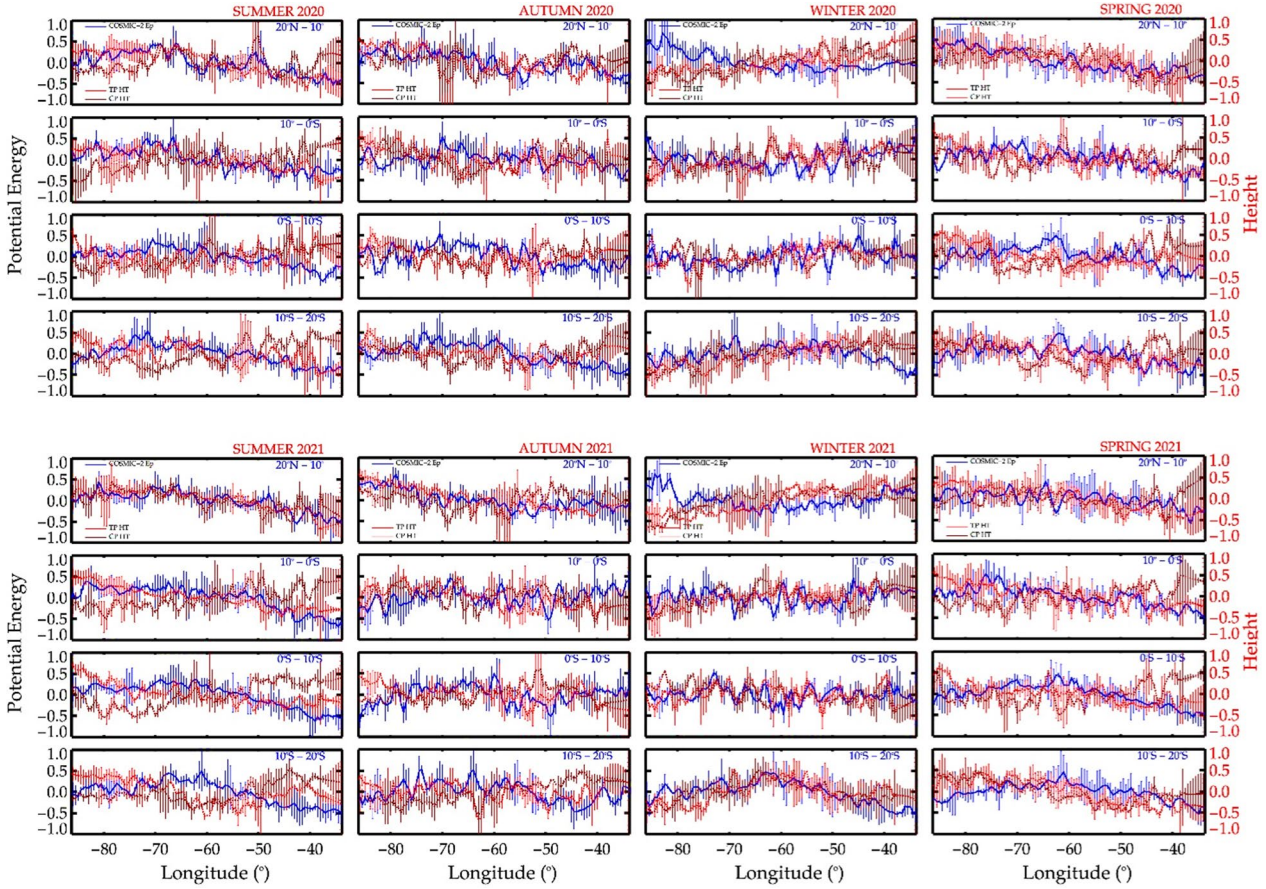

Fig. 9 The seasonal relationship between the latitudinal mean normalized E_p distribution (blue line), TPH (brown dotted line), and CPH (red dotted line) with the error bars for 20°N–10°N, 10°N–0°, 0°–10°S, 10°S–20°S. Each panel shows the mean E_p distribution, TPH, and CPH at 20–30 km altitude

in the tropics and the non-similarity in the subtropics does not necessarily mean correlation and anti-correlation, our focus was not to investigate the relationships between the tropopause parameters. From Fig. 9, the SGW and the tropopause parameters (TPH and CPH) showed interchanging trends in the summer, autumn, and spring. In the tropical winter, the SGW showed mostly, that there is no relationship with the tropopause parameter temperature at Lat1 and Lat 2 (20°N–10°N, 10°S–20°S), and over the Andes at Lat 5 (20°S–30°S). These results are consistent with the findings of Randel et al. (2000); Santer et al. (2003) and Schmidt et al. (2008a). Also, exceptions are seen: there is a strong negative correlation with CPH (2020) in LAT1, there are weak negative correlations with TPH (2020) and CPH (2021) in LAT1, and there is a good and strong positive correlation with TPH (2021) and CPH (2021) in LAT4. These exceptions need to be investigated further.

The CPH generally showed negative or no correlation in all the seasons across the latitudinal divisions in 2020 and 2021. There were four cases where there were positive correlations: first, at $20^oN - 10^oN$ in the summer and spring of 2020 with $r = 0.22$ and 0.49, respectively. Also, at $20^oN - 10^oN$ in 2021 summer with $r = 0.63$. Secondly, at $20^oS - 10^oS$ in the winter with $r = 0.74$. Yu et al. (2019) also observed that the distributions of statistically significant correlation coefficients between GW Ep and lapse rate temperature/height and cold point tropopause temperature/height characteristics were dispersed across the tropics. In autumn, good and strong correlations between SGW, PWV, and TPH were observed in the summer at $20^oN - 10^oN$ in 2020 and 2021. In summary, there are considerable relationships between convection and tropopause characteristics, indicating that low and cold tropopause emerge in deep convection zones in most seasons. Thus, in the tropics, both deep

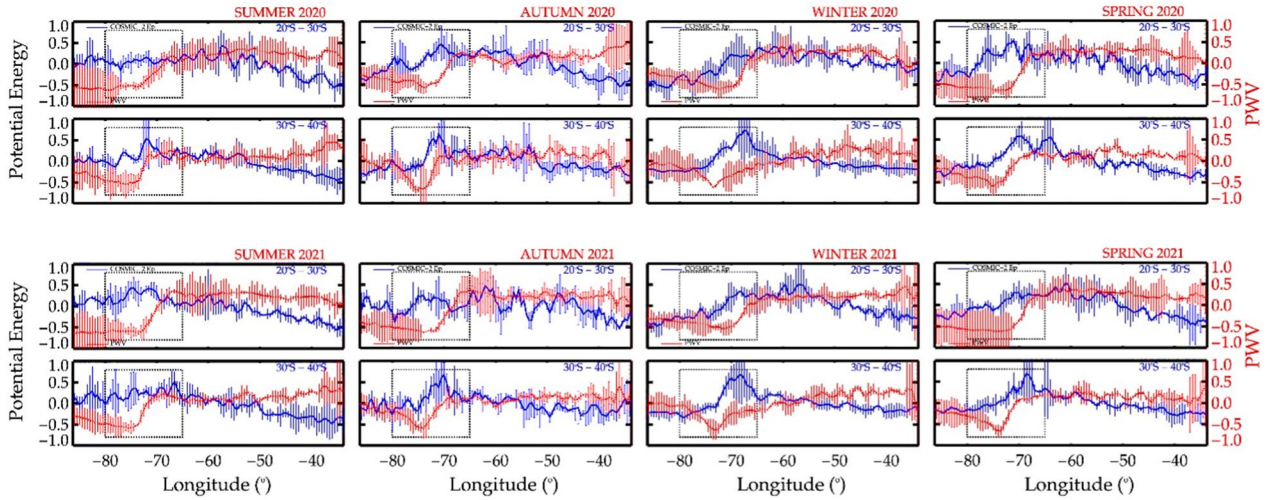

Fig. 10 The seasonal relationship between the latitudinal mean normalized E_p distribution (blue line) and the water vapour (PWV) (red line) with the error bars for 20°S–30°S, and 30°S–40°S. Each panel shows the mean E_p distribution and the PWV at 20–30 km altitude

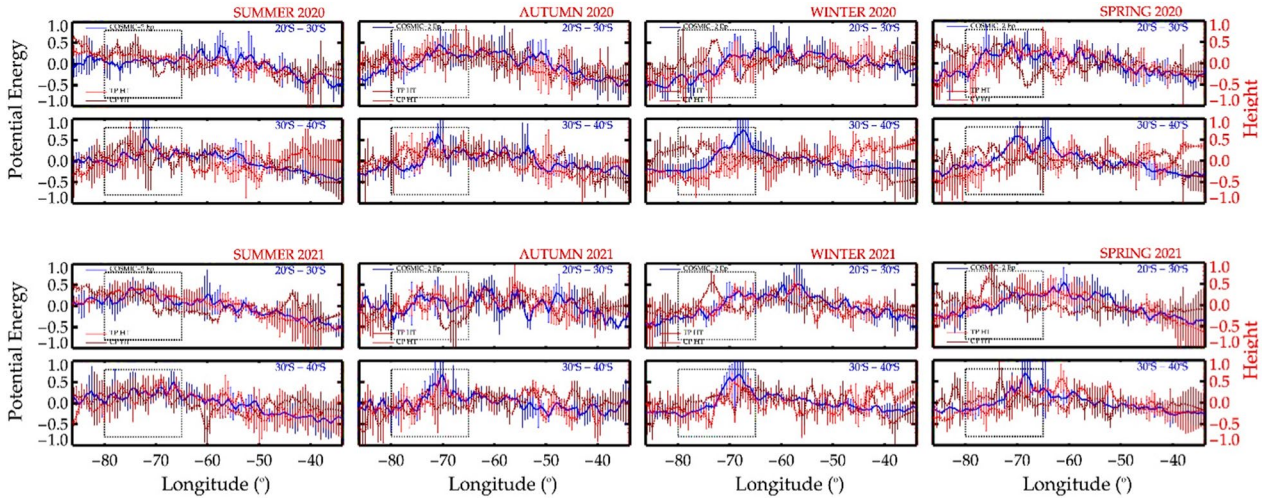

Fig. 11 The seasonal relationship between the latitudinal mean normalized E_p distribution (blue line), TPH (brown dotted line), and CPH (red dotted line) with the error bars for 20°S–30°S, and 30°S–40°S. Each panel shows the mean E_p distribution, TPH, and CPH at 20–30 km altitude

convection and SGWs are influenced by the tropopause structure.

Potential energy vs tropospheric parameters over the Andes

In this section, we analyzed the latitudinal variation of SGW E_p and the tropospheric parameters (PWV, TPH, and CPH) and their respective correlation coefficients over the Andes during the years 2020 and 2021. The latitudinal ranges are divided into two, namely: 20^o S–30^o S and 30^o S—40^o S. The area of interest is marked with the black-dotted rectangular box in Figs. 10 and 11. At 20^o S–30^o S over the Andes Mountains (70^o W–80^o W), the SGWs and the PWV relationship showed an opposite trend, which does not necessarily signify an anti-correlation. Over the Andes mountains at 20^o S–30^o S showed that there is a positive correlation in the summer ($r = 0.38$ and 0.78 in 2020 and 2021, respectively). There are good and strong correlations between the SGW and tropospheric parameters in the summer and spring at 20^o S–30^o S over the Andes Mountains except in the 2021 summer and 2020 spring with no correlation. Contrary to the correlation result over the tropics, the CPH showed relative significance in the 2020 summer, autumn, 2021 winter, and spring over the Andes at 20^o S–30^o S.

At 30^o S–40^o S over the Andes Mountain region, the PWV showed a negative correlation in summer, winter, and a weak correlation in the transitional seasons (autumn $r = 0.13$ (PWV 2020, MAM) and spring $r = 0.26$ (PWV 2021, SON)) in 2020 and 2021. There is strong correlation between the SGW and TPH in the transitional seasons over the Andes Mountain range (Table 2). In winter, our result showed a negative correlation ($r = -0.78$ and $r = -0.35$,) in 2020 and 2021, respectively. This result showed that the lower the water vapour content over the Andes the more the gravity wave activities in the stratosphere. In the Andes Mountains region, the water vapour significantly drops, the E_p rises considerably, and the PWV starts to increase from 70°W eastward across the seasons. Also, at 20°S–30°S (Fig. 4), the PWV increases with a significant decrease in the gravity wave E_p at 70°W–30°W. In contrast, the PWV and the gravity wave E_p showed a similar trend at 30°S–40°S of 70^o W–80^o W in the summer and winter seasons. In the autumn and spring, we found the correlation coefficients at Lat6 to be weak/no correlation in 2020 ($r = 0.13$&$r = 0$) and weak negative/positive correlation in 2021 ($r = -0.25$&$r = 0.26$), respectively.

In these regions, a descending trend is observed from west to east in both E_p and PWV. This could be due to the northern and southern trade winds blowing westward. Zhang et al. (2018) observed that the changes in PWV suggest atmospheric water vapour is strongly tied to the supply of water vapour (oceans and seas) and heat (surface temperature). The PWV variations are complex because it is unclear how these two factors interact to produce water vapour in the high atmosphere. In the latitudinal range of 20°S - 30°S and 30°S - 40°S there was an anti-correlation between the E_p and PWV over the Andes mountains and after the Andes mountains towards the east in the winter. Also, Zhang et al. (2018) observed a much smaller PWV in the midlatitude, with higher values in summer than in other seasons.

At 30°S–40°S (Lat6), our result showed that the SGW E_p is mostly positively correlated with CPH across the seasons. However, there were exceptions in the summer ($r = -0.24$ in CPH 2021), autumn ($r = -0.17$ in CPH 2021), and winter ($r = -0.06$ in CPH 2020). The TPH mostly showed a positive correlation (Table 2) with the SGW Ep in the autumn and spring, and negative correlations in the winter in both years." ($r = -0.75$ in summer in 2020). However, we also found a negative correlation in the summer at Lat6 TPH 2020 ($r = -0.42$) and a positive correlation in the winter at Lat5 TPH 2021 ($r = 0.62$). Our findings are consistent with those of Alexander et al. (2008), who determined that the mean E_p exceeds 2.4 J kg^{-1} in the Himalayas and Eastern China during the winter.

In Fig. 11, there is a clear variation between TPH and CPH over the Andes Mountain at Lat6 ($30°S - 40°S$). The CPH at Lat6 showed an interchanging correlation coefficient in the summer and winter in 2020 and 2021. A strong positive correlation (0.9&0.8) and a weak negative (-0.24& -0.06) correlation in the summer and winter of 2020 and 2021, respectively. A weak positive correlation occurred in the spring of 2020 and 2021. In the autumn, there is a strong/weak positive correlation in 2020/2021. The TPH showed a positive correlation with SGW E_p in the autumn and spring, while it was negatively correlated in the summer and winter.

Discussion

The perturbations of atmospheric temperature caused by SGW activity are shown in Figs. 2 and 3. COSMIC RO temperature profiles are based on the estimation of temperature perturbations (T') in order to calculate the SGW E_p. The illustration provided by Xu et al. (2017) shows that the COSMIC temperature profile varies in the tropopause and throughout the stratosphere. The GPS/MET temperature profiles show this variability as well (Randel et al. 2003; Tsuda et al. 2000). These temperature profile variations may be linked to SGWs, demonstrating that SGWs can influence tropopause temperatures. SGWs have been discovered to be critical in controlling the tropopause's characteristics (Khan and Jin 2016). The tropopause's characteristics are influenced by the breaking of SGWs in the stratosphere, which transport energy, momentum, chemical, and atmospheric elements (such as water vapour) across the tropopause to the surrounding environment (Yu et al. 2019). According to (Salby 1996; Khan and Jin 2016; Yu et al. 2019), the TPH and CPH exhibit unique properties in response to gravity wave transmission in the stratosphere.

Our results in Figs. 8 and 9 showed a positive correlation in the summer, autumn, and spring with a negative correlation in the winter between the tropospheric parameters and the SGW, with several exceptions widely noted in the result section. These exceptions have to be further investigated. This interesting result shows that the PWV may not be responsible for the excitation of SGWs in the winter due to low convective activity shifting towards the northern hemisphere in the winter (Yu et al. 2019). Yu et al. (2019) observed a correlation between convections and tropopause temperature and height, indicating that low and cold tropopause occur in deep convection areas (equator or tropics) and that both deep convections and gravity waves affect tropopause structure. The TPH and CPH variations may be linked to SGWs, indicating that gravity waves may impact tropopause temperature (Khan and Jin 2018). SGWs have been shown to be critical in controlling tropopause

properties. Gravity waves breaking in the stratosphere transfer energy and atmospheric elements through the tropopause to the surroundings, modifying the tropopause parameters in the process (Wang 2003).

As previously shown, gravity waves move PWV and other atmospheric elements from the troposphere to the stratosphere (Wang 2003; Lane and Sharman 2006). The SGW activity is intensified over the Andes mountains during the winter season, reducing PWV defusing into the stratosphere. When SGWs propagate and break, they not only transfer energy and momentum but also vertical mixing of heat, directly or indirectly impacting the tropopause height. PWV and trace gases (e. g., aerosols) are defused into the stratosphere, increasing the concentration of PWV above the cold point height (Yu et al. 2019). As seen in Figs. 2 and 3, the spatial distributions of seasonal gravity wave E_p in the winter and summer are very similar to those seen in Faber et al. (2013) in June-July-August (JJA) and December- January-February (DJF). Higher gravity wave E_p values are seen in winter compared with the summer in extratropical areas (over the Andes and the Patagonian mountains) due to orographic and zonal wind effects. In the other global satellite, climatological studies of gravity waves such as AIRS, the same seasonal occurrence of gravity wave activities attributed to various sources has been linked to convection, orographic generation, wind shear, body forces, and frontal systems (Gong et al. 2012; Hoffmann et al. 2013). Figs. 2 and 3 indicate that gravity wave E_p is higher in the Southern Andes, as seen in previous studies in the winter (Yan et al. 2010; Faber et al. 2013).

In the tropics, there is a strong correlation between convection and tropospheric parameters, indicating that tropopause height appears in deep convection regions, as shown in Fig. 9 and Table 1. The results are consistent with those of Gettelman et al. (2002); Randel and Jensen (2013). Although this correlation could be due to convective cooling of the tropopause or another factor, the former appears to be more likely. Figure 8, on the other hand, shows that in deep convection regions, the correlations between SGW E_p and PWV and temperature are significant, implying that tropopause parameter variability may be related to SGW activity. Randel and Jensen (2013) suggest that radiative forcing might be important for the tropical tropopause, which could be influenced by both deep convection and the SGWs generated by deep convection.

Our results in Figs. 10 and 11 over the Andes Mountain range agreed with (Khan and Jin 2016) who revealed the SGWs influence on the water vapour concentration in the stratosphere. Water vapour, CPT, and gravity wave E_p have a strong relationship with each other above the cold points, and water vapour rises with rising gravity wave E_p. SGWs created by mountains have an effect on mesoscale circulations by carrying energy and momentum from the lower troposphere to the lower and higher stratosphere and balancing their momentum and energy (Fritts and Alexander 2003). Additionally, it was claimed that gravity waves are generated primarily by topography, frontal activity, wind shear, the jet stream, convection, and cyclones. Mountain waves are quasi-stationary and propagate vertically upwards, which shows that the north-south alignment could be favorable to the propagation of the mountain waves (Alexander et al. 2010). A consistent increase in the SGW activities seen in the total mean SGW E_p percentage in Fig. 4 could be attributed to the aid of the mean zonal wind blowing eastward (Alexander et al. 2008; Faber et al. 2013).

Conclusion

In this study, the relationship between the activities of SGW, measured by the dry temperature profile to get the SGW Ep, and the tropospheric parameters TPH, CPH, and PWV is studied and analyzed. We investigate the correlation coefficients of SGW E_p independently with the PWV, TPH, and CPH. The SGW E_p climatology showed little or no evidence of gravity wave activities in the summer at mid-latitudes. Our result showed little or no gravity wave activity during winter in the tropical region at $30-40$ km; this phenomenon is suspected to be wave filtering in the middle stratosphere. The gravity wave E_p increases in winter along with altitude over the Andes Mountains, which could be attributed to the increase in wind intensity, aiding the increase in gravity wave activity. We found that the gravity wave in winter and spring showed a consistent increase from the lower to the upper stratosphere.

Our result showed that PWV is concentrated in the tropical region and mainly in the equatorial region in all seasons. The PWV is higher in the summer and lower in the winter. Most of the PWV is over land, especially the Amazon rain forest. Relatively, good correlations were found between the PWV and the SGW Ep in the tropical summer and spring, while weak/negative correlation coefficients occurred in the winter with some exceptions. The CPH showed a general lack of correlation or anti-correlation with SGW over the South American tropics, with few positive correlations, and a few exceptions. Over the Andes at $20°S-30°S$, an averagely positive correlation between the PWV and Ep occurred in the summer, autumn, and spring. Over the Andes at $30°S-40°S$, strong negative correlations were found in the summer and winter. The TPH's negative/positive correlation with

SGW E_p showed that SGW activities had more impact on the tropopause parameters than the CPH. Therefore, with these exceptions, a definite impact of the gravity wave activities on the CPH could not be ascertained from our analysis. The TPH and PWV showed similar correlations with SGW rather than the CPH. The vertical mixing of heat that occurs during the propagation and breaking of SGWs has an impact on the tropopause height either directly or indirectly. It could be concluded that the gravity waves in the stratosphere over tropical South America and the Andes Mountain range are correlated with the tropospheric parameters. In the tropics, both deep convection and SGWs had a corresponding influence on the tropopause structure; however, at higher latitudes, the tropopause height displayed more fluctuation when GWs propagated from the troposphere to the stratosphere.

Acknowledgements
The authors acknowledged CDAAC for providing the data. We also acknowledge the financial support provided by the Brazilian Ministry of Science, Technology, and Innovations (MCTI) and the Brazilian Space Agency (AEB) and the Conselho Nacional de Desenvolvimento Cient´ıfico e Tecnol´ogico (CNPQ).

Author contributions
For research articles with several authors, a short paragraph specifying their individual contributions must be provided. The following statements should be used "conceptualization, ATT, WCM, and TH; methodology, ATT; software, ATT; validation, WCM, and TH; formal analysis, ATT; investigation, ATT; resources, CDAAC; data curation, ATT; writing—original draft preparation, ATT; writing— review and editing, WCM, TH, FCAOB; visualization, BD, LSO, EP and ABV; supervision, WCM, and TH; project administration, ATT; funding acquisition, WCM.

Funding
The Brazilian Ministry of Science, Technology, and Innovations (MCTI) and the Brazilian Space Agency (AEB), grant number 20VB.0009 and the Conselho Nacional de Desenvolvimento Cientıfico e Tecnol´ogico (CNPQ) with the process number 141373*/2019-9*.

Availability of data and materials
The data used in this study is exclusively provided by CDAAC and they were obtained from http://cdaac-www.cosmic.ucar.edu/cdaac.

Declarations

Competing interests
The authors declare that there is no competing interests or state.

Author details
[1]Space Weather Division, National Institute for Space Research (INPE), Sao Jose Dos Campos, SP, Brazil. [2]School of Built Environment (SBE), University of Environment and Sustainable Development (UESD), Somanya, Eastern Region, Ghana. [3]Department of Physics, Meteorology and Atmospheric Research Lab, University of Cape Coast, Cape Coast, Ghana.

Received: 6 December 2022 Accepted: 26 August 2023
Published online: 11 September 2023

References

Abraham A, Dutta P, Mandal JK, Bhattacharya A, Dutta S (2018) Emerging technologies in data mining and information security. In Proceedings of IEMIS-2018. Springer

Alexander S, Tsuda T, Kawatani Y, Takahashi M (2008) Global distribution of atmospheric waves in the equatorial upper troposphere and lower stratosphere: COSMIC observations of wave mean flow interactions. J Geophys Res Atmos. https://doi.org/10.1029/2008JD010039

Alexander SP, Klekociuk AR, Tsuda T (2009) Gravity wave and orographic wave activity observed around the antarctic and arctic stratospheric vortices by the COSMIC 'GPS-RO satellite constellation. J Geophys Res Atmos. https://doi.org/10.1029/2009JD011851

Alexander P, Luna D, Llamedo P, de la Torre A (2010) A gravity waves study close to the Andes mountains in Patagonia and Antarctica with GPS radio occultation observations. Ann Geophys 28(2):587–595

Baumgaertner AJG, McDonald AJ (2007) A gravity wave climatology for antarctica compiled from challenging minisatellite payload/global positioning system (CHAMP/GPS) radio occultations. J Geophys Res. https://doi.org/10.1029/2006JD007504

Baumgarten K, Gerding M, Baumgarten G, Lubken F-J (2018) Temporal variability of tidal and gravity waves during a record long 10-day continuous lidar sounding. Atmos Chem Phys 18(1):371–384

Cai X, Yuan T, Liu H-L (2017) Large-scale gravity wave perturbations in the mesopause region above northern hemisphere midlatitudes during autumnal equinox: a joint study by the usu na lidar and whole atmosphere community climate model. Ann Geophys 35(2):181–188

Das SS, Kumar KK, Uma K (2010) Mst radar investigation on inertia-gravity waves associated with tropical depression in the upper troposphere and lower stratosphere over gadanki (13.5° n, 79.2° e). J Atmos Solar-terr Phys 72(16):1184–1194

De la Torre A, Alexander P, Llamedo P, Menendez C, Schmidt T, Wickert J (2006) Gravity waves above the andes detected from GPS radio occultation temperature profiles: jet mechanism? Geophys Res Lett. https://doi.org/10.1029/2006GL027343

Faber A, Llamedo P, Schmidt T, de la Torre A, Wickert J (2013) On the determination of gravity wave momentum flux from GPS radio occultation data. Atmos Meas Tech 6(11):3169

Fritts DC, Alexander MJ (2003) Gravity wave dynamics and effects in the middle atmosphere. Rev Geophys. https://doi.org/10.1029/2001RG000106

Fueglistaler S, Dessler AE, Dunkerton TJ, Folkins I, Fu Q, Mote PW (2009) Tropical tropopause layer. Rev Geophys 47:RG1004

Gettelman A, Salby M, Sassi F (2002) Distribution and influence of convection in the tropical tropopause region. J Geophys Res Atmos. https://doi.org/10.1029/2001JD001048

Gisinger S, Polichtchouk I, Dornbrack A, Reichert R, Kaifler B, Kaifler N, Rapp M, Sandu I (2022) Gravity-wave-driven seasonal variability of temperature differences between ECMWF ifs and Rayleigh lidar measurements in the lee of the southern Andes. J Geophys Res Atmos 127(13):e2021JD036270

Gong J, Wu DL, Eckermann S (2012) Gravity wave variances and propagation derived from airs radiances. Atmos Chem Phys 12(4):1701–1720

Hei H, Tsuda T, Hirooka T (2008) Characteristics of atmospheric gravity wave activity in the polar regions revealed by GPS radio occultation data with CHAMP. J Geophys Res Atmos 113(17):463–473

Held IM, Hou AY (1980) Nonlinear axially symmetric circulations in a nearly inviscid atmosphere. J Atmos Sci 37(3):515–533

Hierro R, Llamedo P, De La Torre A, Alexander P, Rolla A (2012) Climatological patterns over South America derived from COSMIC radio occultation data. J Geophys Res Atmos. https://doi.org/10.1029/2011JD016413

Hoffmann L, Xue X, Alexander M (2013) A global view of stratospheric gravity wave hotspots located with atmospheric infrared sounder observations. J Geophys Res Atmos 118(2):416–434

Jain AR, Das SS, Mandal TK, Mitra AP (2006) Observations of extremely low tropopause temperature over the Indian tropical region during monsoon and post monsoon months: possible implications. J Geophys Res Atmos 111(D7):1–16

Khan A, Jin S (2016) Effect of gravity waves on the tropopause temperature, height and water vapor in Tibet from cosmic GPS radio occultation observations. J Atmos Solar Terr Phys 138:23–31

Khan A, Jin S (2018) Gravity wave activities in Tibet observed by COSMIC 'GPS radio occultation. Geodesy Geodyn 9(6):504–511

Kim J, Son S-W (2012) Tropical cold-point tropopause: climatology, seasonal cycle, and intraseasonal variability derived from COSMIC GPS radio occultation measurements. J Clim 25(15):5343–5360

Kishore P, Namboothiri S, Igarashi K, Jiang JH, Ao CO, Romans LJ (2006) Climatological characteristics of the tropopause parameters derived from GPS/CHAMP and GPS/SAC-C measurements. J Geophys Res Atmos. https://doi.org/10.1029/2005JD006827
Lane TP, Sharman RD (2006) Gravity wave breaking, secondary wave generation, and mixing above deep convection in a three-dimensional cloud model. Geophys Res Lett. https://doi.org/10.1029/2006GL027988
Liu X, Yue J, Xu J, Wang L, Yuan W, Russell JM III, Hervig ME (2014) Gravity wave variations in the polar stratosphere and mesosphere from SOFIE/AIM temperature observations. J Geophys Res Atmos 119(12):7368–7381
Randel WJ, Wu F (2005) Kelvin wave variability near the equatorial tropopause observed in GPS radio occultation measurements. J Geophys Res Atmos. https://doi.org/10.1029/2004JD005006
Randel WJ, Jensen EJ (2013) Physical processes in the tropical tropopause layer and their roles in a changing climate. Nat Geosci 6:169–176
Randel WJ, Wu F, Rios WR (2003) Thermal variability of the tropical tropopause region derived from gps/met observations. J Geophys Res 108:4024–4024
Randel WJ, Wu F, Gaffen DJ (2000) Interannual variability of the tropical tropopause derived from radiosonde data and NCEP reanalyzes. J Geophys Res Atmos 105(D12):15509–15523
Ratnam MV, Tetzlaff G, Jacobi C (2004) Global and seasonal variations of stratospheric gravity wave activity deduced from the CHAMP/GPS satellite. J Atmos Sci 61(13):1610–1620
Reid GC, Gage KS (1981) On the annual variation in height of the tropical tropopause. J Atmos Sci 38(9):1928–1938
Salby ML (1996) Fundamentals of atmospheric physics. Elsevier, Amsterdam
Santer BD, Sausen R, Wigley TML, Boyle JS, Achutarao K, Doutriaux C, Hansen JE, Meehl GA, Roeckner E, Ruedy R, Schmidt G, Taylor KE (2003) Behavior of tropopause height and atmospheric temperature in models, reanalyses, and observations: decadal changes. J Geophys Res 108:4002. https://doi.org/10.1029/2002JD002258
Satheesan K, Murthy BK (2005) Modulation of tropical tropopause by wave disturbances. J Atmos Solar Terr Phys 67(10):878–883
Scherllin-Pirscher B, Steiner AK, Anthes RA, Alexander MJ, Alexander SP, Biondi R, Birner T, Kim J, Randel WJ, Son S-W et al (2021) Tropical temperature variability in the UTLS: New insights from GPS radio occultation observations. J Clim 34(8):2813–2838
Schmidt T, Wickert J, Beyerle G, Reigber C (2004) Tropical tropopause parameters derived from GPS radio occultation measurements with champ. J Geophys Res Atmos. https://doi.org/10.1029/2004JD004566
Schmidt T, Beyerle G, Heise S, Wickert J, Rothacher M (2006) A climatology of multiple tropopauses derived from gps radio occultations with champ and sac-c. Geophys Res Lett. https://doi.org/10.1029/2005GL024600
Schmidt T, De La Torre A, Wickert J (2008) Global gravity wave activity in the tropopause region from champ radio occultation data. Geophys Res Lett. https://doi.org/10.1029/2008GL034986
Schmidt T, Wickert J, Beyerle G, Heise S (2008b) Global tropopause height trends estimated from GPS radio occultation data. Geophys Res Lett 35(11):1473–1488
Schreiner W, Weiss J, Anthes R, Braun J, Chu V, Fong J, Hunt D, Kuo Y-H, Meehan T, Serafino W, Sjoberg J, Sokolovskiy S, Talaat E, Wee T, Zeng Z (2020) Cosmic-2 radio occultation constellation: First results. Geophys Res Lett 47(4):e2019GL086841
Seidel DJ, Randel WJ (2006) Variability and trends in the global tropopause estimated from radiosonde data. J Geophys Res Atmos. https://doi.org/10.1029/2006JD007363
Seidel DJ, Ross RJ, Angell JK, Reid GC (2001) Climatological characteristics of the tropical tropopause as revealed by radiosondes. J Geophys Res 106:7857–7878
Son S-W, Tandon NF, Polvani LM (2011) The fine-scale structure of the global tropopause derived from COSMIC 'GPS radio occultation measurements. J Geophys Res 116:D20113
Strelnikova I, Almowafy M, Baumgarten G, Baumgarten K, Ern M, Gerding M, Lubken F-J (2021) Seasonal cycle of gravity wave potential energy densities from lidar and satellite observations at 54° and 69° n. J Atmos Sci 78(4):1359–1386
Teng W-H, Huang C-Y, Ho S-P, Kuo Y-H, Zhou X-J (2013) Characteristics of global precipitable water in ENSO events revealed by COSMIC measurements. J Geophys Res Atmos 118(15):8411–8425
Tsuda T, Nishida M, Rocken C, Ware RH (2000) A global morphology of gravity wave activity in the stratosphere revealed by the 'GPS occultation data (GPS/MET). J Geophys Res Atmos 105(5):7257–7273
Wang PK (2003) Moisture plumes above thunderstorm anvils and their contributions to cross-tropopause transport of water vapor in midlatitudes. J Geophys Res 108:4194
Wang J, Zhang L (2008) Systematic errors in global radiosonde precipitable water data from comparisons with ground-based GPS measurements. J Clim 21(10):2218–2238
Wang L, Alexander MJ (2009) Gravity wave activity during stratospheric sudden warmings in the 2007–2008 northern hemisphere winter. J Geophys Res Atmos 114(1):1235–1238
Wang L, Alexander M (2010) Global estimates of gravity wave parameters from GPS radio occultation temperature data. J Geophys Res Atmos. https://doi.org/10.1029/2010JD013860
Xian T, Fu Y (2015) Characteristics of tropopause-penetrating convection determined by TRMM and COSMIC GPS radio occultation measurements. J Geophys Res Atmos 120(14):7006–7024
Xu X, Yu D, Luo J (2017) Seasonal variations of global stratospheric gravity wave activity revealed by COSMIC RO data. In 2017 Forum on Cooperative Positioning and Service (CPGPS), pages 85–89. IEEE
Yan X, Arnold N, Remedios J (2010) Global observations of gravity waves from high resolution dynamics limb sounder temperature measurements: A yearlong record of temperature amplitude and vertical wavelength. J Geophys Res Atmos. https://doi.org/10.1029/2008JD011511
Yang S-S, Pan C-J, Das U (2021) Investigating the spatio-temporal distribution of gravity wave potential energy over the equatorial region using the era5 reanalysis data. Atmosphere 12(3):311
Yu D, Xu X, Luo J, Li J (2019) On the relationship between gravity waves and tropopause height and temperature over the globe revealed by COSMIC radio occultation measurements. Atmosphere 10(2):75
Zhang Y, Xu J, Yang N, Lan P (2018) Variability and trends in global precipitable water vapor retrieved from cosmic radio occultation and radiosonde observations. Atmosphere 9(5):174
Zhou X, Holton JR (2002) Intraseasonal variations of tropical cold-point tropopause temperatures. J Clim 15(12):1460–1473

Publisher's Note